

11-1-2023

A laser-based Angstrom method for in-plane thermal characterization of isotropic and anisotropic materials using infrared imaging

A. Gaitonde

A. Candadai

Justin A. Weibel
jaweibel@purdue.edu

A. M. Marconnet

Follow this and additional works at: <https://docs.lib.purdue.edu/coolingpubs>

Gaitonde, A.; Candadai, A.; Weibel, Justin A.; and Marconnet, A. M., "A laser-based Angstrom method for in-plane thermal characterization of isotropic and anisotropic materials using infrared imaging" (2023). *CTRC Research Publications*. Paper 410.
<http://dx.doi.org/https://doi.org/10.1063/5.0149659>

This document has been made available through Purdue e-Pubs, a service of the Purdue University Libraries. Please contact epubs@purdue.edu for additional information.

RESEARCH ARTICLE | JULY 17 2023

A laser-based Ångström method for in-plane thermal characterization of isotropic and anisotropic materials using infrared imaging

Aalok U. Gaitonde ; Aaditya A. Candadai ; Justin A. Weibel ; Amy M. Marconnet  



Rev. Sci. Instrum. 94, 074904 (2023)

<https://doi.org/10.1063/5.0149659>



View
Online



Export
Citation

CrossMark

Articles You May Be Interested In

Nanoconfined catalytic Ångström-size motors



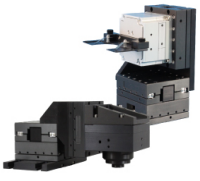
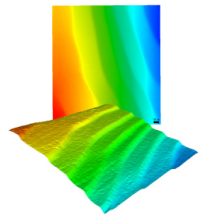
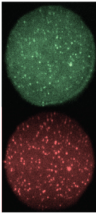
J. Chem. Phys. (November 2015)

Fast Fourier transform Ångström method for fast thermal measurements of microfibers

Rev. Sci. Instrum. (January 2023)

Microplasma emission spectroscopy of carbon dioxide using the carbon monoxide Ångström system

J. Appl. Phys. (February 2020)

 MCL MAD CITY LABS INC. www.madcitylabs.com	<p>Nanopositioning Systems</p> 	<p>Modular Motion Control</p> 	<p>AFM and NSOM Instruments</p> 	<p>Single Molecule Microscopes</p> 
---	--	--	---	--

A laser-based Ångstrom method for in-plane thermal characterization of isotropic and anisotropic materials using infrared imaging

Cite as: Rev. Sci. Instrum. 94, 074904 (2023); doi: 10.1063/5.0149659

Submitted: 7 March 2023 • Accepted: 29 June 2023 •

Published Online: 17 July 2023



View Online



Export Citation



CrossMark

Aalok U. Gaitonde,  Aaditya A. Candadai,  Justin A. Weibel,  and Amy M. Marconnet^{a)} 

AFFILIATIONS

The Birck Nanotechnology Center and The School of Mechanical Engineering, Purdue University, 585 Purdue Mall, West Lafayette, Indiana 47907, USA

^{a)} Author to whom correspondence should be addressed: marconnet@purdue.edu

ABSTRACT

High heat fluxes generated in electronics and semiconductor packages require materials with high thermal conductivity to effectively diffuse the heat and avoid local hotspots. Engineered heat spreading materials typically exhibit anisotropic conduction behavior due to their composite construction. The design of thermal management solutions is often limited by the lack of fast and accurate characterization techniques for such anisotropic materials. A popular technique for measuring the thermal diffusivity of bulk materials is the Ångstrom method, where a thin strip or rod of material is heated periodically at one end, and the corresponding transient temperature profile is used to infer the thermal diffusivity. However, this method is generally limited to the characterization of one-dimensional samples and requires multiple measurements with multiple samples to characterize anisotropic materials. Here, we present a new measurement technique for characterizing the isotropic and anisotropic in-plane thermal properties of thin films and sheets as an extension of the one-dimensional Ångstrom method and other lock-in thermography techniques. The measurement leverages non-contact infrared temperature mapping to measure the thermal response from laser-based periodic heating at the center of a suspended thin film sample. Uniquely, our novel data extraction method does not require precise knowledge of the boundary conditions. To validate the accuracy of this technique, numerical models are developed to generate transient temperature profiles for hypothetical anisotropic materials with known properties. The resultant temperature profiles are processed through our fitting algorithm to extract the in-plane thermal conductivities without knowledge of the input properties of the model. Across a wide range of in-plane thermal conductivities, these results agree well with the input values. Experiments demonstrate the approach for a known isotropic reference material and an anisotropic heat spreading material. The limits of accuracy of this technique are identified based on the experimental and sample parameters. Further standardization of this measurement technique will enable the development and characterization of engineered heat spreading materials with desired anisotropic properties for various applications.

Published under an exclusive license by AIP Publishing. <https://doi.org/10.1063/5.0149659>

NOMENCLATURE

A	amplitude of steady periodic temperature oscillations	k_y	thermal conductivity in the lateral or in-plane y -direction
c_p	specific heat	k_z	thermal conductivity in the through-thickness z -direction
f	frequency of heating	n	number of grid points or pixels
H	sample thickness	P	real part of the complex temperature amplitude
h	convective heat transfer coefficient	q''	heat flux
k_x	thermal conductivity in the lateral or in-plane x -direction	Q	imaginary part of the complex temperature amplitude
		r	radius
		T	temperature

t	time
α	thermal diffusivity
ρ	density
ω	angular frequency of heating
ϕ	phase delay

I. INTRODUCTION

The development and discovery of new materials is a primary enabler of technological breakthroughs.¹ Over the past decade, research efforts have led to the creation of unique thin films,² polymer fibers and composites,^{3,4} and battery materials.^{5,6} Such newly developed materials possess advantageous properties for various applications ranging from energy to health to electronics.

A specific interest in thermal engineering applications has been the broad potential impact of advanced materials with extreme and tunable thermal conductivity for both thermal insulation and heat spreading applications.⁷⁻⁹ For example, recent work has demonstrated several forms of graphene and carbon-nanotube (CNT)-based films and sheets with ultra-high thermal conductivity for heat dissipation from electronic devices. Xin *et al.*¹⁰ fabricated large-area graphene sheets having a thermal conductivity greater than $1200 \text{ W m}^{-1} \text{ K}^{-1}$ using a roll-to-roll process, demonstrating far superior hotspot dissipation compared to conventional heat spreaders. Yu *et al.*¹¹ designed super-aligned CNT films with different alignment configurations, achieving tunable in-plane and cross-plane thermal conductivities. Two-dimensional nanomaterials such as few-layer black phosphorus have been shown to exhibit in-plane thermal anisotropy, providing guidance for the design of optoelectronic devices.¹² There is also great interest in the development of high thermal conductivity polymer fibers and composites for dielectric, flexible, and wearable heat spreading applications.^{13,14} Such materials inherently possess in-plane anisotropy with respect to thermal properties due to the directional alignment and orientation of polymer chains.¹⁵⁻¹⁷ Xu *et al.*¹⁸ fabricated ultra-drawn, highly oriented polyethylene films with a thermal conductivity of up to $62 \text{ W m}^{-1} \text{ K}^{-1}$ along the direction of the drawing. Our recent work¹⁹ demonstrated the construction of high in-plane thermal conductivity fabrics using woven yarns of ultra-high molecular weight polyethylene fiber, yielding a fabric with a thermal conductivity of up to $\sim 10 \text{ W m}^{-1} \text{ K}^{-1}$ along the high packing density direction. It was predicted that the effective thermal conductivity can range from ~ 2 to $10 \text{ W m}^{-1} \text{ K}^{-1}$ based on the directional packing density, indicating the potential to tune the in-plane thermal anisotropy for such fabrics.

In light of these recent material advancements, the development of complementary experimental measurement methods for the characterization of in-plane anisotropic thermal properties becomes essential. There are only a few recent studies that have demonstrated the measurement of in-plane anisotropic thermal conductivity.^{12,20,21} For few-layer black phosphorous, Luo *et al.*¹² utilized micro-Raman spectroscopy to measure the anisotropic thermal conductivity. Modified versions of the time-domain thermoreflectance (TDTR) technique have also recently been used to measure in-plane thermal anisotropy.^{20,21} Such techniques are limited to measuring very thin film materials ($<10\text{--}100 \mu\text{m}$) and require complex and expensive optical systems.

The Ångström method^{22,23} and the laser-flash method^{24,25} are two other popular measurement techniques that can be used to measure the thermal properties of materials with simpler equipment. In the standard laser-flash method, a short pulse of energy heats one side of a flat sample uniformly, while the transient temperature rise of the opposite face is measured by a detector. This temperature profile is then used to calculate the thermal diffusivity of the sample. This technique assumes one-dimensional heat transfer across the thickness of the sample, and is generally limited to the measurement of the through-thickness thermal conductivity of bulk materials. This laser-flash technique can be adapted to measure the in-plane thermal diffusivity of materials by applying a ring shaped heating profile to one side of the sample, and measuring the transient temperature rise of the opposite side at the center of the ring.^{26,27} In the Ångström method, one end of a long, thin strip of material is heated periodically, and the measurement of the temperature oscillations and phase delay at two different locations along the sample length can be used to extract the material's thermal diffusivity. The analysis involves fitting the experimental temperature measurements to a one-dimensional heat transfer model to calculate thermal diffusivity. Recent studies, such as those by Hahn *et al.*,²⁸ Kim *et al.*,²⁹ and Hu and Fisher,³⁰ have focused on making this technique more versatile, accurate, and scalable to smaller sample dimensions with non-contact infrared microscopy-based measurements of temperatures. However, all prior Ångström methods are limited to measurements along a single direction and require multiple strips to determine the anisotropy of the material along different directions. Therefore, there is a need to develop a measurement technique that enables in-plane thermal characterization of anisotropic materials across a range of different types and forms of materials.

A few techniques have explored the use of lock-in infrared thermography for the measurement of thermophysical properties of thin films and plates by using the response of the material to periodic heating. Welch *et al.*³¹ presented a technique where a pulsating laser heat source is rasterized across a sample surface, and the temperature of the backside of the sample is measured using IR thermography. Perez and Autrique³² and Mendioroz *et al.*³³ used a similar approach where periodic heating was achieved using halogen lamps and suitable optics. Kato *et al.*³⁴ developed a technique based on lock-in thermography, where temperature measurements are performed using thermocouples. While some of these techniques are capable of measuring in-plane thermal anisotropy, they involve moving the heat source across the sample using optical and mechanical apparatus and assuming uniform absorption of the laser radiation across the surface. This assumption may not be true for samples that may have varying surface properties, such as those of composite materials. Some of these methods are limited to measuring low anisotropy ratios in the in-plane direction,³² while others can only resolve anisotropy across the in-plane and through-plane directions.³⁴ More recently, in-plane thermal conductivity has been measured using a beam-offset frequency domain thermoreflectance (FDTR) technique.³⁵ Such techniques are capable of measuring the full thermal conductivity tensor for transversely anisotropic materials. However, they are typically limited to measuring an in-plane anisotropy ratio of up to ~ 10 . It has also been reported that the measurement uncertainty for low conductivity materials can be influenced by the pump beam radius and lateral heat spreading in

the thin metallic transducer layer that needs to be applied for such thermoreflectance-based methods.^{35–37}

Here, we develop and validate a new characterization technique to quantify the anisotropic in-plane thermal properties of freestanding thin films and sheets of material. A laser periodically heats the sample at one fixed central point, while infrared (IR) microscopy measures the resulting two-dimensional in-plane temperature field in a non-contact fashion. The proposed technique builds upon the principles of our recent demonstration of an IR-enhanced Ångström method²⁸ and translates them into a multi-dimensional analysis with the ability to characterize in-plane anisotropic thermal properties of materials such as thin heat spreaders, composite films, and fabrics across a wide range of thermal conductivities and anisotropy ratios. The principle of this technique, its experimental implementation, and associated numerical models for the extraction of the desired material properties are detailed in the following sections.

II. MEASUREMENT TECHNIQUE

A. Experimental configuration

The measurement technique developed here extends the principles of the Ångström method to two dimensions in order to extract the in-plane thermal properties of a material based on the measured temperature response when subjected to periodic heating. The basic principle of the one-dimensional Ångström method is that the amplitude and phase lag of the time-periodic temperature oscillations in the material are sensitive to thermal diffusivity. An extension of this principle to an in-plane two-dimensional temperature

distribution is proposed to allow in-plane anisotropic thermal property characterization for sample geometries such as films, sheets, and fabrics. We leverage a discretized form of the heat diffusion equation in the frequency domain evaluated throughout the spatial domain to extract the unknown thermal properties from the measured time-periodic material temperature distribution (without solving the differential equation). Since the thermal property extraction is based on the amplitude of oscillations and phase lag of the temperature signals, this measurement is independent of the laser power, the periodic heating frequency, or the precise boundary condition at the edge of the suspended sample. The method introduced here targets the measurement of the in-plane anisotropic thermal properties, with the anisotropy defined based on different thermal conductivities along the orthogonal directions.

Figure 1(a) shows a schematic of the experimental setup. The sample is suspended over a cylindrical hole in a heat sink that maintains the outer portion of the sample contacting the fixture close to room temperature (or the temperature of the fluid flowing through the heat sink). A small central spot on the bottom surface of the sample is heated using a laser beam. A laser driver connected to a function generator provides a modulated square-wave periodic heat input. The transient time-periodic temperature response of the entire top surface of the sample is measured using an infrared camera. A thin graphite-coated circular metal disk is attached via adhesive to the bottom surface of the sample to act as an absorber for the incident laser beam. The absorber serves several practical purposes: (1) to absorb a large fraction of the incident laser power regardless of sample surface properties; (2) to ensure the heated

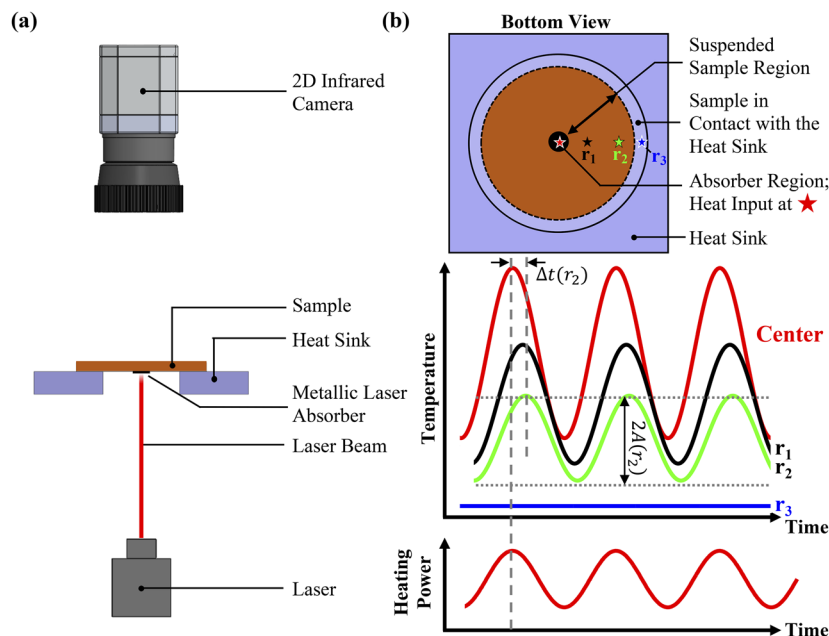


FIG. 1. (a) Schematic of the conceptual setup for the laser-based Ångström method. Periodic heat input is applied to the center of the bottom surface of a suspended sample using a laser source, and the two-dimensional transient temperature distribution of the top surface of the sample is measured using an IR camera. (b) Bottom view of the sample and illustration of the time-periodic temperature response at four different points at increasing distances away from the location of the periodic laser heat input. The heating power corresponds to the first harmonic of the square wave profile applied to the laser source.

area is approximately circular, mitigating the effect of any eccentricity of the beam spot; and (3) to prevent any laser radiation from transmitting through the sample and damaging the infrared detector. In principle, for fully opaque samples, the absorber disk can be eliminated. This experimental setup allows for non-contact temperature sensing in the suspended sample region. It should be noted that the laser beam remains stationary and that the laser irradiation is incident on a fixed point on the laser absorber throughout the experiment.

During the measurement, the sample is heated at a set frequency and power that are controlled using a frequency generator and by adjusting the power of the laser, respectively. The sample temperature response is then allowed to reach a steady periodic state, after which the temperature is recorded as a function of space and time. Typically, ~5–10 periods of temperature oscillation are recorded to perform the subsequent data analysis. As illustrated in Fig. 1(b), the temperature response gradually decreases in amplitude and increases in phase delay, as illustrated by the time delay in the peaks, Δt , with increasing distance from the point of laser incidence. While the figure shows a sinusoidal heating power, experimentally, we often use a square wave heating signal for the simplicity of controlling the laser. Then, using Fourier transforms, the amplitude and phase of the first harmonic of the temperature response, which has the highest amplitude, are analyzed to extract thermal conductivity. Assuming that the temperature dependence of thermal conductivity has a negligible effect within the range of temperature oscillations, the form of the heat source profile has minimal influence on estimating thermal conductivity. In Sec. II B, we describe how the experimental data are combined with an associated thermal analysis to yield the in-plane thermal properties of the sample.

B. Data analysis for property extraction

This section presents the data analysis method used to extract the thermal properties of a sample from the steady, periodic temperature response. This is an inverse method that determines the unknown in-plane thermal properties that cause the temperature response to best satisfy the governing heat conduction equations. Notably, the method does not require knowledge of laser power input, through-plane thermal conductivity, or the temperature of the heat sink boundary condition to extract the in-plane anisotropic thermal conductivity.

1. General 2D approach for characterizing anisotropic materials

This method analyzes the transient two-dimensional temperature profile, $T(x, y, t)$, of the top surface of the sample in the suspended domain between the edge of the metal absorber disk and the edge of the heat sink, as shown in the bottom view of the schematic in Fig. 1(b). The temperature response must satisfy the governing heat diffusion equation assuming 2D in-plane heat conduction,

$$\frac{\partial}{\partial x} \left(k_x \frac{\partial T}{\partial x} \right) + \frac{\partial}{\partial y} \left(k_y \frac{\partial T}{\partial y} \right) = \rho C_p \frac{\partial T}{\partial t}. \quad (1)$$

This form of the equation allows for thermal conductivity to differ in the in-plane coordinate directions as $k = k_x \hat{x} + k_y \hat{y}$. This analysis

also assumes, by the nature of a two-dimensional conduction equation, that the temperature is uniform across the sample thickness, such that k_z does not factor into the analysis. As the temperature data analyzed are collected under steady periodic conditions, a time-periodic temperature solution is assumed for the suspended domain, which can be written in the complex form in the frequency domain as

$$T(x, y, t) = [P(x, y) + iQ(x, y)]e^{i\omega t}, \quad (2)$$

where $P(x, y)$ and $Q(x, y)$ represent the real and imaginary parts of the complex amplitude, and $e^{i\omega t}$ accounts for the periodic behavior of the solution, with $\omega = 2\pi f$ representing the angular frequency of the periodic heat input. Substituting this general solution for temperature into Eq. (1) and equating the real and imaginary parts, we obtain the following set of partial differential equations for P and Q :

$$k_x \frac{\partial^2 P}{\partial x^2} + k_y \frac{\partial^2 P}{\partial y^2} = -\rho C_p \omega Q, \quad (3)$$

$$k_x \frac{\partial^2 Q}{\partial x^2} + k_y \frac{\partial^2 Q}{\partial y^2} = \rho C_p \omega P. \quad (4)$$

The above equations are valid at each pixel in the suspended portion domain without heat generation (i.e., in the region between the outer edge of the absorber disk and the edge of the heat sink). They can be solved as simultaneous algebraic equations based on the computation of the second order partial derivatives for P and Q locally at each point in the domain from the experimental data to obtain a map of $k_x(x, y)$ and $k_y(x, y)$. Alternatively, assuming that the material should be homogeneous through the domain, these can also be solved as a system of algebraic equations across all the points inside the domain, say n points, as shown below:

$$\begin{bmatrix} \frac{\partial^2 P_1}{\partial x^2} & \frac{\partial^2 P_1}{\partial y^2} \\ \dots & \dots \\ \dots & \dots \\ \frac{\partial^2 Q_1}{\partial x^2} & \frac{\partial^2 Q_1}{\partial y^2} \\ \dots & \dots \\ \dots & \dots \end{bmatrix}_{2n \times 2} \begin{bmatrix} k_x \\ k_y \end{bmatrix} = \rho C_p \omega \begin{bmatrix} -Q_1 \\ \dots \\ \dots \\ P_1 \\ \dots \\ \dots \end{bmatrix}_{2n \times 1}. \quad (5)$$

The steady periodic temperature response of the sample $T_{\text{exp}}(x, y, t)$ is processed using a Fourier transform at each point in the domain to obtain the in-phase and out-of-phase components at the fundamental frequency (frequency of periodic heating), which correspond to the spatially varying real (P) and imaginary (Q) parts of the temperature amplitude signal at each pixel. To reduce uncertainty in the measurement, a magnitude threshold (typically 0.5–1 °C) is defined for the amplitude of oscillation, and any data points in the domain where the temperature amplitude is below this threshold are omitted from the analysis (see the supplementary material, Sec. S2). Using the built in *gradient* operator in MATLABTM, the second-order partial derivatives of P and Q with respect to x and y are computed numerically. To reduce the amplification of spatial noise in the calculated partial derivatives,

a convolution filter is applied between successive gradient operations using a square kernel of a size ranging from 5×5 to 11×11 pixels. Data can be processed at any chosen collection of points in the domain to fit single values of k_x and k_y using Eq. (5) that best fit their collective temperature response. This analysis is implemented using the MATLAB *Optimization Toolbox*, which calculates the quantities k_x and k_y such that it minimizes the objective function given by $\| [PQ] \cdot [k] - [pq] \|$, where $[PQ]$ represents the coefficient matrix on the left hand side of Eq. (5), $[pq]$ represents the matrix on the right hand side of Eq. (5), $[k]$ represents the orthotropic thermal conductivity matrix, and $\|$ denotes the Euclidean norm. Note that in the absence of explicit knowledge of ρ and c_p , Eq. (5) can be divided by the term ρc_p , and the thermal diffusivity values α_x and α_y can be fitted directly. This approach for extracting property information from the data is similar to that presented by Christov *et al.*³⁸

As noted above, the approach is valid assuming the temperature gradients along the through-thickness direction of the sample in the region analyzed are negligible compared to the gradients in the in-plane direction. An advantage of this approach is that the boundary conditions do not need to be specifically measured or accounted for in the model, provided that the region of analysis does not closely approach the boundaries. Hence, the points chosen to fit the in-plane thermal conductivities in the current configuration must be sufficiently far away from the inner heating and outer heat sink boundary conditions. The validity of these assumptions depends on various parametric considerations relating to the sample and the measurement setup, which are further discussed in the supplementary material, Sec. S3.

2. 1D radial approach for isotropic materials

For the general case of an anisotropic material, the transient heat diffusion equation has no simple analytical solution, and the two-dimensional data analysis technique described in Sec. II B 1 must be used. However, if the thermal conductivity in the in-plane direction is isotropic, an analytical solution for the temperature response in radial coordinates can also be used to infer the thermal conductivity from the measurement data. The model of the linear-Ångstrom method described by Hahn *et al.*²⁸ can be extended to a radial coordinate system to determine the in-plane thermal diffusivity (and, therefore, thermal conductivity) of the sample using an analytical approach.

The one-dimensional transient heat diffusion equation in radial coordinates is given below:

$$\frac{\partial^2 T}{\partial r^2} + \frac{1}{r} \frac{\partial T}{\partial r} = \frac{1}{\alpha} \frac{\partial T}{\partial t}. \quad (6)$$

The boundary conditions considered are temperature oscillations in a complex form with fixed amplitudes T_a and T_b at two respective radial locations $r = a$ and $r = b$ inside the sample domain and a phase lag ϕ_b between them,

$$T(r = a, t) = \frac{T_a}{2} e^{i\omega t} + \frac{T_a}{2} e^{-i\omega t}, \quad (7)$$

$$T(r = b, t) = \frac{T_b}{2} e^{i(\omega t - \phi_b)} + \frac{T_b}{2} e^{-i(\omega t + \phi_b)}. \quad (8)$$

Note that such boundary conditions can be selected at multiple radial locations due to the availability of high-resolution transient temperature data throughout the sample surface from IR imaging.

A general periodic solution for the temperature profile in the frequency domain can be written as

$$T(r, t) = T_1(r) e^{i\omega t} + T_2(r) e^{-i\omega t}. \quad (9)$$

Here $T_1(r)$ and $T_2(r)$ represent general complex functions that can be solved by substituting back into the governing equation and are in the form of Bessel functions, J_0 and Y_0 , of the periodic heating frequency ω and the in-plane thermal diffusivity α , respectively. Therefore, an analytical solution for the temperature profile can be obtained if the parameters T_a , T_b , and ϕ_b are known. These parameters can be taken from the experimental data for a given sample of interest to obtain an analytical solution of the steady periodic radial temperature profile. The unknown in-plane thermal diffusivity α of the sample (and, hence, thermal conductivity k) is determined by fitting the analytical solution to the experimental temperature profile at a given periodic heating frequency based on the steady periodic amplitude $A(r)$ and phase $\phi(r)$ of the temperature oscillations. A fitting function that combines $A(r)$ and $\phi(r)$ of the form $f((r - r_0)^2) = \ln \frac{A_0}{A(r)} (\phi_0 - \phi(r))$, similar to that used by Hahn *et al.*²⁸ for a linear system, yields the thermal diffusivity of the sample.

C. Experimental facility

An experimental facility is developed to demonstrate this measurement technique. Figure 2(a) shows a cross-section view of a three-dimensional drawing of the experimental assembly, while Fig. 2(b) shows a photograph of the assembled setup. The sample is sandwiched between two copper plates with holes in the center that expose the top and bottom sides of the suspended sample. The bottom copper plate has an annular O-ring groove, which aids in removing slack from flexible or thin samples using compression of an O-ring placed in this groove. The bottom copper plate is secured to a temperature-controlled aluminum mounting plate. Temperature control, if required to characterize heat sink temperatures above/below ambient, is achieved by circulating fluid of a known temperature from a chiller through internal channels in the mounting plate.

After the sample is mounted between the copper plates, it is coated with a thin layer of colloidal graphite (Ted Pella, Inc., Iso-propanol Base Graphite) having an emissivity of ~ 0.8 for purposes of IR imaging. A graphite-coated, thin aluminum disk (cut from an adhesive tape with an aluminum substrate) is attached at the center of the bottom sample face to absorb the incident laser power and provide a uniform, circular heat source. In principle, for high-emissivity and opaque samples, these steps (graphite coating and transducer attachment) are not necessarily required.

The suspended sample is heated periodically with a fiber-coupled diode laser (BWTek BWF2, 980 nm, max 5 W continuous wave) from the bottom. A square wave laser heating profile at the desired frequency is achieved by modulating the laser output using a function generator. The output laser fiber is secured rigidly to the aluminum mounting plate using a threaded sub-miniature version-A (SMA) adapter to ensure alignment of the laser heat source to the center of the sample under test.

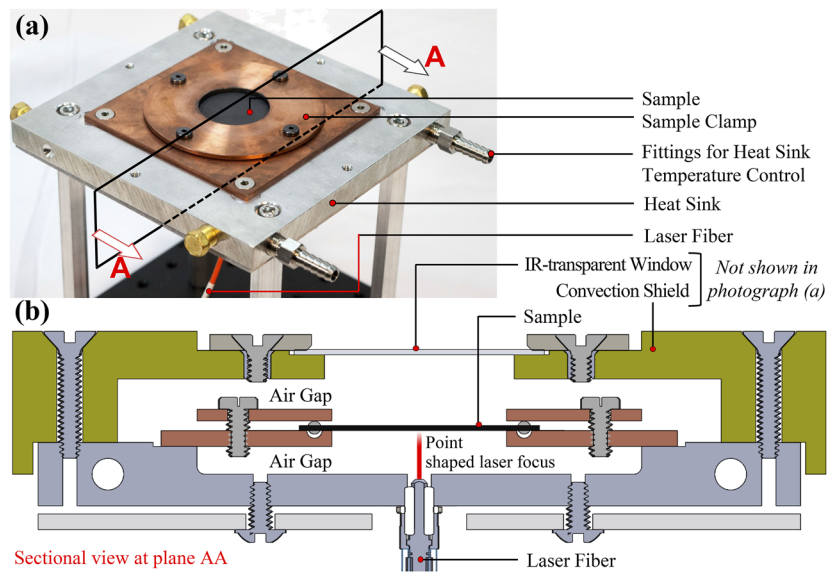


FIG. 2. (a) Photograph of the experimental facility (without the convection shield), highlighting the salient features. (b) Sectional view of the experimental facility at cut-plane AA shows the sample (black) sandwiched between two copper plates, which are fastened to a temperature-controlled heat sink. The fiber output from the diode laser is secured to the mounting plate using an adapter threaded into the heat sink that aligns the laser beam with the center of the sample. To reduce the effects of convection, a 3-D printed shield may be placed on top of the experimental facility to reduce convective losses from the sample during experiments. An IR transparent Calcium Fluoride (CaF_2) window allows thermal imaging through the shield. Note that there is an air gap between the sample surface and the shield, and the CaF_2 window is not in thermal contact with the sample or the sample clamp.

The assembly may be enclosed from above by an additively-manufactured polymer shield to minimize the convective losses from the sample during experiments. The shield houses a Calcium Fluoride (CaF_2) window, which is nearly fully transparent across the 2–5 μm infrared spectrum, matching the range of the IR microscope detector sensitivity. Note that neither the convection shield nor the CaF_2 window are in thermal contact with the sample, and there exists an air gap between the shield and the sample. This arrangement enables the temperature measurements of the top surface of the sample to be performed using an IR camera. In this work, an infrared microscope (InfrascopeTM, Quantum Focus Instruments Corporation) is used. The interchangeable lenses on this microscope allow for measurements at various spatial resolutions, with an imaging field of view of 1024×1024 pixels. For the measurements reported in this work, a $1/6\times$ magnification infrared lens is used, which corresponds to a spatial resolution of $\sim 75 \mu\text{m}/\text{pixel}$ and provides a sufficiently large field of view of $\sim 77 \times 77 \text{ mm}^2$ to measure the surface temperature response of the sample.

III. NUMERICAL EXPERIMENTS FOR MEASUREMENT TECHNIQUE VALIDATION

A. Introduction to numerical experiments

To validate the proposed measurement technique and guide the design of the experimental facility, a numerical thermal conduction model of the system is developed to generate simulated data. These so-called “numerical experiments” are performed using COMSOLTM Multiphysics, as further described below.

A 3D model geometry containing the salient features of the experimental setup in which thermal conduction must be simulated, including the suspended sample and an aluminum heat sink with a cylindrical hole, is modeled with appropriate boundary conditions as shown in Fig. 3(a). A thin aluminum disk of 5 mm diameter is attached to the bottom surface of the sample. Note that neither the absorption properties of this material nor the contact resistance between the disk and the sample are important, as the in-plane thermal properties of the sample are determined only from the transient thermal response of the sample in the suspended domain away from the heat source and heat sink and independent of exact knowledge of the heat input or absorbed laser power. A periodic heat flux condition is assigned to the central $\sim 1 \text{ mm}$ diameter region of the aluminum disk in the form $q''(t) = q_o''(1 + \sin(2\pi ft))$, where q_o'' is the laser heat flux, f is the periodic heating frequency, and t is time. A fixed temperature boundary condition is assigned to the aluminum heat sink.

The material properties of the sample, including its density ρ , specific heat C_p , and anisotropic thermal conductivity (k_x , k_y , and k_z), are specified as inputs to the model. Here, k_x and k_y represent the thermal conductivities along the x and y in-plane orthotropic directions, while k_z represents the through-plane thermal conductivity.

The output of the numerical experiments is the simulated transient temperature data exported from the top surface of the sample at a regular grid of points that mimics the spatial temperature data collected by the infrared microscope. As illustrated by the data processing workflow shown in Fig. 3(b), the numerical experiments provide a transient surface temperature map $T_{\text{exp}}(x, y, t)$ similar to what would be measured in a real experiment. This dataset can then

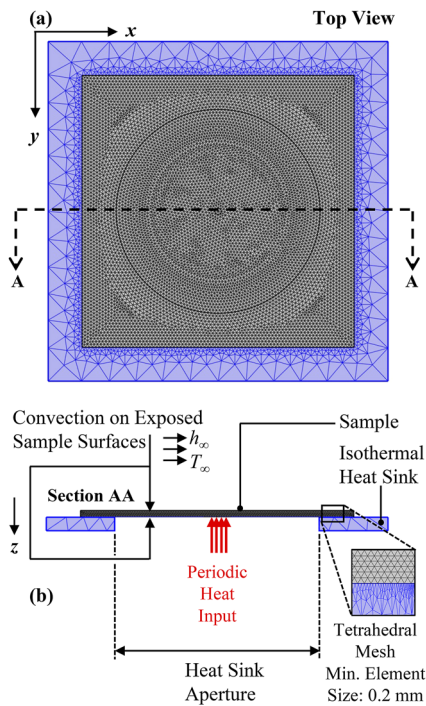


FIG. 3. Overview of the numerical experiments: (a) Top view of the meshed geometry and (b) a vertical section of the model with labeled boundary conditions assigned to the components for performing numerical experiments.

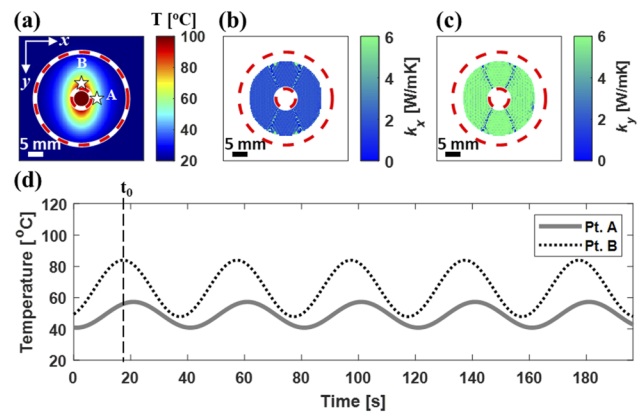


FIG. 4. Representative analysis of numerical simulations for a sample with in-plane anisotropic thermal conductivity: $k_x = 2 \text{ W m}^{-1} \text{ K}^{-1}$ and $k_y = 6 \text{ W m}^{-1} \text{ K}^{-1}$. (a) Top surface temperature map from the numerical simulations at a time instant t_0 during the steady periodic temperature oscillations. (b) $k_x(x, y)$ and (c) $k_y(x, y)$ obtained individually at each point in the domain. The dashed circles indicate the inner and outer boundaries, representing the edge of the laser absorber and the edge of the heat sink. (d) Evolution of temperature with time at points A and B. The temperature profile along the low conductivity x -direction at A shows a decay in the temperature and phase delay compared to the temperature evolution at B along the high conductivity y -direction.

be processed using the data analysis method introduced in Sec. II B 1 for the extraction of the in-plane thermal conductivities of the sample, k_x and k_y . The extracted properties can then be compared to the numerical model inputs to validate that the proposed measurement technique can determine the orthotropic in-plane thermal conductivities of a material, independent of its through-plane conductivity and input power.

In Sec. III B, the results of the proposed measurement method and the data analysis approach are presented by analyzing representative numerical experiments for anisotropic and isotropic materials.

B. Measurement validation for an anisotropic material

A fictitious in-plane anisotropic sample that is $500 \mu\text{m}$ thick with thermal conductivities $k_x = 2 \text{ W m}^{-1} \text{ K}^{-1}$, $k_y = 6 \text{ W m}^{-1} \text{ K}^{-1}$, and $k_z = 0.5 \text{ W m}^{-1} \text{ K}^{-1}$, density $\rho = 970 \text{ kg m}^{-3}$, and specific heat capacity $c_p = 1950 \text{ J kg}^{-1} \text{ K}^{-1}$ is considered. Numerical experiments are performed using this sample, and the data are analyzed using the general 2D approach as described in Sec. II B 1. The input heat flux is $q_0' = 5 \times 10^5 \text{ W m}^{-2}$ at a frequency of $f = 25 \text{ mHz}$, and a total of 25 periods with 100 time steps in each period are simulated.

A snapshot of the instantaneous temperature distribution taken at time t_0 over the top surface of the sample, extracted on a square grid from the simulation results, is shown as a contour plot in Fig. 4(a). The elliptical isotherms, with higher temperatures at the same distance away from the center in the y -direction compared to

the x -direction, indicate the in-plane anisotropy of the sample. The two inner and outer dashed circles represent the boundaries of the domain, corresponding to the edges of the metal disk absorber and the edge of the heat sink platform, respectively. The transient temperatures at two points A and B, equidistant from the center of the sample, are plotted in Fig. 4(d). The transient profile shown here is the steady, periodic temperature response of the material due to the periodic nature of the laser heat input. The temperature profile at point B displays a higher mean temperature and amplitude of oscillations due to the three-times higher in-plane thermal conductivity along the y -direction.

The transient temperature data are used to extract the spatially varying real and imaginary parts of the complex temperature amplitude, P and Q , at each point on the grid, as described in Sec. V. These are then used to simultaneously solve the discretized forms of Eqs. (3) and (4) to obtain a map of thermal conductivities k_x and k_y at each grid point, which are plotted in Figs. 4(b) and 4(c), respectively. Grid points within and near the boundary conditions, such as those inside the region of the absorber and those close to the inner dashed circle (generally within a radial distance 6–7 times the laser spot radius), are excluded from the analysis. In addition, points near the outer dashed circle are also excluded due to the intrinsic noise present in the numerical gradient approximation that becomes significant near boundaries where the geometry and mesh change. These excluded grid points are illustrated in white in Figs. 4(b) and 4(c).

For the calculated maps of k_x and k_y shown, the average extracted values across all analyzed grid points are $k_x = 2.01 \text{ W m}^{-1} \text{ K}^{-1}$ and $k_y = 6.13 \text{ W m}^{-1} \text{ K}^{-1}$. However, the calculated standard deviations are high (>100% in each case) due to the nature of the point-by-point computation. At several individual points, the extracted k_x and k_y have high errors, as apparent from the contour plots in Figs. 4(b)

and 4(c) that skew the standard deviations. Therefore, while these contour maps are useful to graphically illustrate the computed values of thermal conductivity at each point in the domain, we ultimately consider and recommend a single fit of k_x and k_y based on the collective data analysis approach as presented in Eq. (5). Considering all the included points in the domain to extract single values based on Eq. (5) yields $k_x = 1.98 \text{ W m}^{-1} \text{ K}^{-1}$ and $k_y = 6.22 \text{ W m}^{-1} \text{ K}^{-1}$ with 95% confidence intervals of (1.975, 1.987) and (6.208, 6.234), respectively. Therefore, for this fictitious anisotropic sample, the in-plane orthotropic thermal conductivities are determined to within 4% of the input values for the numerical simulation model.

C. Measurement validation for an isotropic material

For isotropic materials, numerical experiments are also performed for a sample with equal in-plane orthotropic thermal conductivities of $2 \text{ W m}^{-1} \text{ K}^{-1}$ in both the x and y directions. All other input parameters match the anisotropic validation case described above. In this isotropic case, the instantaneous surface temperature map, the steady periodic transient response, and the point-by-point calculated maps of k_x and k_y are shown in Fig. 5. The in-plane isotropic nature of the sample is evident from the circular isotherms in Fig. 5(a) and the overlapping transient temperature traces in the two different coordinate directions in Fig. 5(d). The extracted values of k_x and k_y based on solving the system of equations [Eq. (5)] are 1.98 and $1.98 \text{ W m}^{-1} \text{ K}^{-1}$ with confidence intervals of (1.975, 1.982) and (1.977, 1.983), respectively. These agree well with the input thermal conductivity values.

This isotropic case enables validation of the proposed generalized 2D approach for property extraction (described in Sec. II B 1) by allowing for a direct comparison with the 1D radial analytical approach (described in Sec. II B 2). The same transient temperature data are processed using the analytical solution approach by

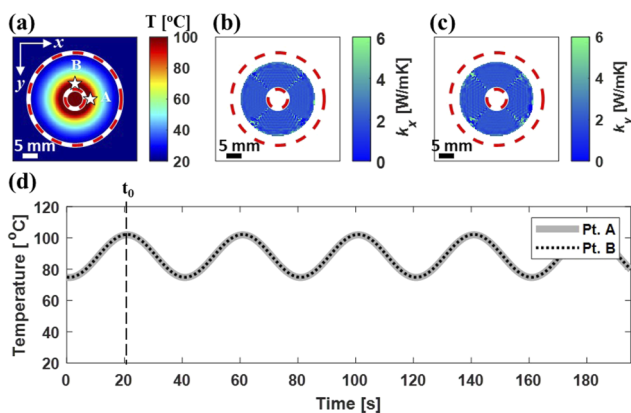


FIG. 5. Representative analysis of numerical simulations for a sample with in-plane isotropic thermal conductivity: $k_x = 2 \text{ W m}^{-1} \text{ K}^{-1}$ and $k_y = 2 \text{ W m}^{-1} \text{ K}^{-1}$. (a) Top surface temperature map from the numerical simulations at a time instant t_0 during the steady-periodic temperature oscillations. Extracted maps of (b) $k_x(x, y)$ and (c) $k_y(x, y)$ obtained individually from calculations at each point in the domain. The inner and outer red-dashed circles indicate the edges of the metal tape laser absorber and the edge of the heat sink, respectively. (d) Evolution of temperature with time at points A and B. The temperature profiles collapse onto each other due to the in-plane isotropy of the material.

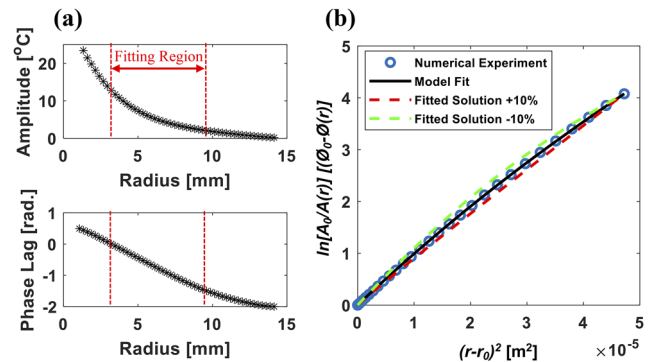


FIG. 6. One dimensional analysis of the isotropic example numerical experiment data for the case of the in-plane isotropic sample with $k_x = 2 \text{ W m}^{-1} \text{ K}^{-1}$ and $k_y = 2 \text{ W m}^{-1} \text{ K}^{-1}$. (a) Temperature amplitude and phase difference as a function of radial distance from the edge of the metal tape disk averaged over 360° . The data from the fitting region between the two vertical red-dashed lines is used to fit for the thermal conductivity of the sample as shown in (b) along with 10% sensitivity bounds. A fitted conductivity of $1.995 \text{ W m}^{-1} \text{ K}^{-1}$ agrees well with the input value of $2 \text{ W m}^{-1} \text{ K}^{-1}$.

obtaining the amplitude and phase lag of the temperature oscillations as a function of the radial distance from the outer radius of the metal tape disk to the edge of the heat sink platform. This is done by dividing this suspended region of the sample into 50 radial segments and averaging the temperature data within these segments over 360° . This spatially averaged temperature amplitude and phase lag data are plotted in Figs. 6(a) and 6(b). As expected, the amplitude of the oscillations continuously decreases with increasing radial distance, and the magnitude of the phase lag (i.e., negative phase difference) also continuously increases with radial distance. By fitting the combined amplitude and phase parameter ϕ (as described in Sec. II B 2) in the region indicated by the vertical red-dashed lines in Fig. 6(a), the thermal diffusivity of the sample is obtained. These dashed lines correspond to the same radial locations shown by the red dashed circles in Fig. 5(a). The fitted result is not significantly dependent on the chosen fitting region in this case, provided the starting point is sufficiently away from the inner boundary for the one-dimensional radial heat transfer assumption to hold. The data from the numerical experiment, fitted result, and 10% sensitivity bounds for the fitted solution are plotted in Fig. 5(b). The fitted thermal diffusivity of $\alpha = 1.06 \times 10^{-6} \text{ m}^2 \text{ s}^{-1}$ corresponds to a thermal conductivity of $1.99 \text{ W m}^{-1} \text{ K}^{-1}$, which agrees well with the input value of $2 \text{ W m}^{-1} \text{ K}^{-1}$ and to the value extracted with the generalized fitting approach.

IV. RESULTS AND DISCUSSION

A. Measurement considerations

The numerical experiments and analysis presented above demonstrate the applicability and validity of the proposed method to characterize the in-plane anisotropic thermal properties of a sample based on the known measured transient temperature distribution of the top surface when subjected to periodic heating. The thermal conductivities in the in-plane direction are extracted independently of the laser heat input and the through-plane sample properties.

The main assumption of the property extraction technique is that the heat transfer is two-dimensional in the plane of the sample and that the through-plane temperature gradient across the sample thickness H is negligible. This assumption is generally valid when the region of analysis does not include locations close to the laser heat input. However, it is important to quantitatively assess the associated limits of this property extraction method, depending on the properties of the sample. In particular, the in-plane vs through-plane thermal properties and the thickness of the sample influence the periodic heating frequency and the dimensions of the experimental setup to be chosen for a particular measurement. By choosing these controllable measurement parameters appropriately, the accuracy of the technique can be maintained over a wide range of thermal properties and length scales.

A primary measurement consideration is the relative through-plane vs in-plane thermal conductance of the sample, which also directly relates to the sample thickness H . To minimize the error induced by through-plane temperature gradients of the sample, a sufficiently low frequency should be used such that the sample thickness is much lower than the thermal penetration depth. This condition can be given as

$$f \ll \frac{\alpha_z}{\pi H^2}, \tag{10}$$

where $\alpha_z = \frac{k_z}{\rho C_p}$. Therefore, for a given through-plane conductivity and sample thickness, the input frequency for accurate measurements should be much smaller (i.e., a factor of ~ 0.1) compared to this upper bound.

Conversely, the frequency of heating cannot be too low and should be sufficiently high to minimize the effect of the boundaries on the in-plane conduction based on the dimensions of the setup. In particular, the temperature oscillation amplitude should be sufficiently attenuated close to the boundaries, such that the change in the amplitude and phase difference across the suspended region is large. This condition has been defined by Hahn *et al.*²⁸ as follows:

$$f \gg \frac{2.98\alpha_{x,y}}{\pi L_s^2}, \tag{11}$$

where $\alpha_{x,y} = \frac{k_{x,y}}{\rho C_p}$ and L_s is the characteristic sample length, which here corresponds to the outer radius of the heat sink platform (characteristic sample length along the radial direction). Depending on the specific sample parameters involved, the measurement frequency can be on the same order as this ideal lower bound.

The recommended frequency bounds of 0.01 and 1 Hz described above are graphically illustrated in Fig. 7 for a specific case corresponding to $k_{x,y} = 4 \text{ W m}^{-1} \text{ K}^{-1}$, $k_z = 0.5 \text{ W m}^{-1} \text{ K}^{-1}$, $H = 500 \text{ }\mu\text{m}$, and $R = 15 \text{ mm}$. The upper measure frequency bound is dictated by the values of k_z and the thickness H , and the lower bound by the values of $k_{x,y}$ and R . In this way, for a given experimental setup, sample geometry, and anticipated thermal properties, the frequency of the periodic heat input can be chosen to lie in the region indicated between these two limits, with an example choice of 25 mHz. This plot serves as a general guideline to assist in the choice of measurement parameters and understand the limits of the measurement. For example, it is observed from the figure that measurements of a sample with high in-plane conductivity ($>100 \text{ W m}^{-1} \text{ K}^{-1}$) and low through-plane conductivity ($<0.1 \text{ W m}^{-1} \text{ K}^{-1}$) would not be feasible for this particular case of sample thickness and outer radius of the setup. This would motivate a measurement facility design change (e.g., a higher R would be needed for such a sample). It is important to note that this plot does not consider the in-plane anisotropy of the sample, a separate and important measurement consideration requiring further analysis to thoroughly understand the complete parametric space associated with this measurement technique.

To demonstrate the tunability of the measurement approach based on the properties of the sample, various numerical experiments are considered with the in-plane orthotropic thermal conductivity of the sample spanning 4 orders of magnitude from 0.2 to $2000 \text{ W m}^{-1} \text{ K}^{-1}$. In each case, the through-plane thermal

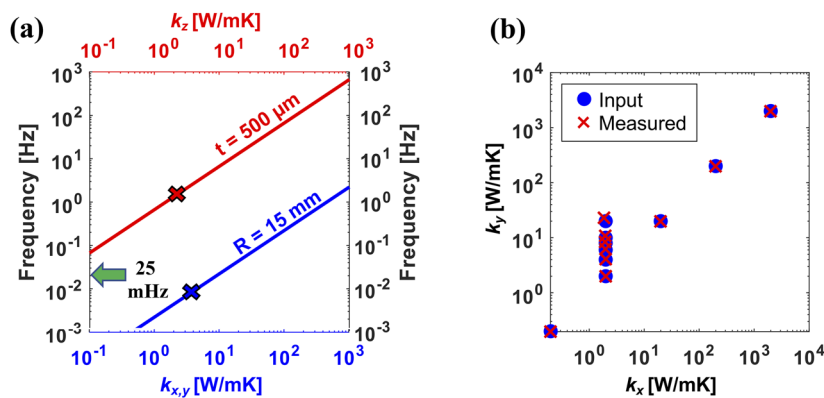


FIG. 7. (a) Illustration of periodic heating frequency bounds depending on the in-plane and through-plane thermal conductivity of a sample at a fixed value of thickness and outer radius of the experimental setup. An example case corresponding to $k_{x,y} = 4 \text{ W m}^{-1} \text{ K}^{-1}$ and $k_z = 0.5 \text{ W m}^{-1} \text{ K}^{-1}$ is depicted as indicated by the pair of \times points, with the recommended heating frequency range of ~ 0.01 to ~ 1 Hz. An example frequency choice (25 mHz) for measurement in this particular case is indicated. (b) Numerical experiment input (O symbols) and extracted (\times symbols) thermal conductivities for a variety of combinations of in-plane orthotropic thermal conductivities along the x and y directions demonstrate the applicability of the proposed measurement method across a wide range of thermal conductivity values.

conductivity is set to be on the order of 10% of the in-plane thermal conductivity as a representative factor of in-plane to through-plane anisotropy. Fixed input values of sample thickness of 0.5 mm, density of 970 kg m^{-3} , and heat capacity of $1950 \text{ J kg}^{-1} \text{ K}^{-1}$ are assumed. Figure 7(b) shows a chart plotting the two in-plane thermal conductivity values against each other over this range, where for each combination the numerical experiment inputs are compared to the extracted properties. For each pair of data points plotted, the input laser power and heating frequency are adjusted following the guidelines above to accurately capture the in-plane thermal conductivities. As an example, a heating power of $5 \times 10^5 \text{ W m}^{-2}$ and a frequency of 25 mHz are used for the case of $k_x, k_y = 2 \text{ W m}^{-1} \text{ K}^{-1}$, while a heating power of $1 \times 10^8 \text{ W m}^{-2}$ at a frequency of 10 Hz is used for the case of $k_x, k_y = 2000 \text{ W m}^{-1} \text{ K}^{-1}$. The agreement between the input and extracted conductivity values is within 1% for cases where $k_x = k_y$ across the broad range of thermal conductivity considered. In addition, for a fixed $k_x = 2 \text{ W m}^{-1} \text{ K}^{-1}$, an in-plane anisotropic ratio of up to 10 ($2 < k_y < 20 \text{ W m}^{-1} \text{ K}^{-1}$) is accurately predicted to within an average error of <10%. The error for anisotropic ratios in the range of 1–8 is within 5% of error, increasing to ~10% for an anisotropic ratio of 10. This increase in error with increasing anisotropy is mainly related to increased relative differences in temperature oscillations and phase lag along the primary in-plane directions, which are captured with lesser accuracy for a given value of heating frequency. Conducting multiple sets of experiments spanning a frequency range and extracting a single property value that best fits the temperature response across this entire range can potentially be used to reduce this error for highly anisotropic (in-plane) materials. However, for the current approach using a single measurement frequency, an anisotropic ratio of 10 can be considered a conservative upper bound; such high anisotropic ratios in the in-plane direction are nevertheless atypical.

B. Effect of convective losses

Another important consideration for this measurement technique is the effect of heat loss due to convection. This can be trivially accounted for in the governing equation by including a heat loss term in Eq. (1),

$$\frac{\partial}{\partial x} \left(k_x \frac{\partial T}{\partial x} \right) + \frac{\partial}{\partial y} \left(k_y \frac{\partial T}{\partial y} \right) - \frac{2h(T - T_\infty)}{H} = \rho C_p \frac{\partial T}{\partial t}, \quad (12)$$

where H is the thickness of the material and h is the heat transfer coefficient assumed to be uniform and constant over both the upper and lower surfaces of the sample. This results in a modified form of the system of governing equations to fit k_x and k_y as

$$\begin{bmatrix} \frac{\partial^2 P_1}{\partial x^2} & \frac{\partial^2 P_1}{\partial y^2} \\ \dots & \dots \\ \dots & \dots \\ \frac{\partial^2 Q_1}{\partial x^2} & \frac{\partial^2 Q_1}{\partial y^2} \\ \dots & \dots \\ \dots & \dots \end{bmatrix}_{2n \times 2} \begin{bmatrix} k_x \\ k_y \end{bmatrix} = \begin{bmatrix} \frac{2hP_1}{H} - \rho C_p \omega Q_1 \\ \dots \\ \dots \\ \frac{2hQ_1}{H} + \rho C_p \omega P_1 \\ \dots \\ \dots \end{bmatrix}_{2n \times 1}. \quad (13)$$

The system of equations can be solved by fitting for k_x and k_y with an input estimate of the convection coefficient, h . Equation (13) also illustrates another tunable aspect of this measurement technique based on the frequency of operation. For a particular sample, depending on the order of sample thermal conductivity, the frequency can be increased such that the term $\frac{2hP_1}{H}$ becomes negligible compared to the term $\rho C_p \omega Q_1$ in Eq. (13). In such a scenario, sample properties can be extracted independent of the effect of convection.

Alternatively, for materials and ambient conditions where the influence of the convective heat transfer coefficient cannot be ignored, all three parameters, k_x , k_y , and h , can be estimated based on a three parameter least squares fit as

$$\begin{bmatrix} \frac{\partial^2 P_1}{\partial x^2} & \frac{\partial^2 P_1}{\partial y^2} & \frac{-2P_1}{H} \\ \dots & \dots & \dots \\ \dots & \dots & \dots \\ \frac{\partial^2 Q_1}{\partial x^2} & \frac{\partial^2 Q_1}{\partial y^2} & \frac{-2Q_1}{H} \\ \dots & \dots & \dots \\ \dots & \dots & \dots \end{bmatrix}_{2n \times 3} \begin{bmatrix} k_x \\ k_y \\ h \end{bmatrix} = \begin{bmatrix} -\rho C_p \omega Q_1 \\ \dots \\ \dots \\ \rho C_p \omega P_1 \\ \dots \\ \dots \end{bmatrix}_{2n \times 1}. \quad (14)$$

Further, if the values of ρ and c_p are unknown, Eq. (14) could be divided by the term ρc_p , and the thermal diffusivity values α_x , α_y , and $(h/\rho c_p)$ can be fitted directly.

C. Experimental characterization and validation

Here, an experimental demonstration of the proposed measurement method is presented for an isotropic and anisotropic material. The isotropic material is a polytetrafluoroethylene (PTFE) sheet, and the anisotropic material is an engineered polymer heat spreading sheet [DupontTM, Temprion[®] Organic Heat Spreader (OHS)³⁹]. While PTFE is a well-known isotropic material, the Temprion[®] OHS material exhibits an extreme case of in-plane anisotropy among available materials. Experimental results for these two materials are described in detail below in Secs. IV C 1 and IV C 2, respectively.

1. Thermal characterization of PTFE

Polytetrafluoroethylene (PTFE) is a common material that has well characterized thermal properties, making it a good candidate for use as a reference material for measurement technique development.^{40,42–45} Figure 8(a) shows the experimentally measured 2D temperature profile in a 500 μm thick PTFE sample at a fixed time instant t_0 , and Fig. 8(b) shows the transient temperature response at two spatial locations A and B for a few heating cycles at steady periodic conditions. Thermal isotropy is not assumed in the measurement analysis, and k_x and k_y are fitted independently. However, because the material is expected to have isotropic thermal properties, the x and y directions are assigned arbitrarily. The density and specific heat of PTFE are $2200 \text{ m}^3 \text{ kg}^{-1}$ and $970 \text{ J kg}^{-1} \text{ K}^{-1}$, respectively.^{40,41} Figure 8 shows the measured thermal conductivity values along the x and y directions as a function of heating frequency. The symbols signify the mean value of thermal conductivity,

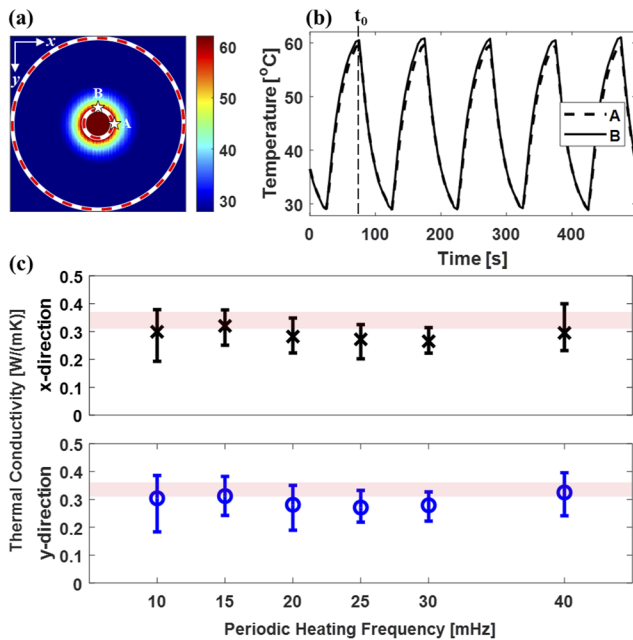


FIG. 8. (a) Two-dimensional temperature distribution on the top surface of the PTFE sample at a time instant t_0 , where the center of the domain attains the highest temperature. (b) Transient temperature response at two discrete locations (Point A on the right edge of the laser absorber and Point B at the top edge of the laser absorber). (c) Experimentally measured values of thermal conductivity in the two in-plane orthotropic directions (k_x and k_y) as a function of the heating frequency. The symbols denote the mean thermal conductivity measured at a particular heating frequency, while the error bars denote the uncertainty in the measurement. The shaded light red horizontal bands represent the expected range of thermal conductivity of PTFE from the literature.^{40,41,42}

while the error bars show the uncertainty in the measurement originating from the thermal image processing and data analysis. The mean values of k_x and k_y are 0.29 ± 0.02 and 0.29 ± 0.03 $\text{W m}^{-1} \text{K}^{-1}$, respectively, approximately centered within the range of the expected thermal conductivity for PTFE,^{40,41} as indicated by the shaded horizontal bands in the figure. The equal values of k_x and k_y confirm the isotropic behavior of this material.

2. Thermal characterization of the anisotropic Dupont Temprion[®] organic heat spreader

The Dupont[™] Temprion[®] Organic Heat Spreader (OHS) material is an electrically insulating flexible polymeric thin film of thickness $45 \mu\text{m}$ that is used for heat spreading applications. It exhibits a high degree of in-plane and through-plane thermal anisotropy. The manufacturer-specified values of thermal conductivity in the three orthotropic directions, k_x , k_y , and k_z , are 0.2, 45, and $0.2 \text{ W m}^{-1} \text{K}^{-1}$, respectively.³⁹ The two in-plane x and y directions are referred to as the *transverse* and *machine* directions, respectively, with z being along the through-plane direction. This translates to an in-plane anisotropy ratio ($k_{\text{machine}}/k_{\text{transverse}}$) of 225. The density and specific heat of this material are $1500 \text{ m}^3 \text{ kg}^{-1}$ and $1000 \text{ J kg}^{-1} \text{K}^{-1}$, respectively (Ref. 46). During characterization, the material was mounted such that the low-conductivity transverse

and high-conductivity machine directions were aligned with the x and y coordinate systems of the thermal imaging sensor on the IR microscope. Figure 9(a) shows a snapshot of the 2D temperature distribution at a single instant. The elliptical isotherms indicate higher thermal diffusion in the y -direction. The corresponding transient temperature profiles for a few time periodic cycles at two points A and B are shown in Fig. 9(b). Note the decay in amplitude of temperature oscillations along the x -direction (dotted black curve) compared to the y -direction (solid black curve). Figure 9(c) shows the experimentally measured values of k_x and k_y across a range of heating frequencies. The mean thermal conductivity in the transverse direction is $k_x = 1.0 \pm 0.3 \text{ W m}^{-1} \text{K}^{-1}$ and in the machine direction is $k_y = 37.5 \pm 2.6 \text{ W m}^{-1} \text{K}^{-1}$ (see the supplementary material, Sec. S1 for quantification of uncertainty in these measurements). Although the measured mean conductivity value in the x -direction is higher than the specification on the data sheet and that in the y -direction is lower, this difference is expected due to the variability in the material itself, which stems from batch-to-batch construction and processing.³⁹ Numerical experiments have also been performed for this material, and the extracted thermal conductivity in the transverse and machine directions agrees well with

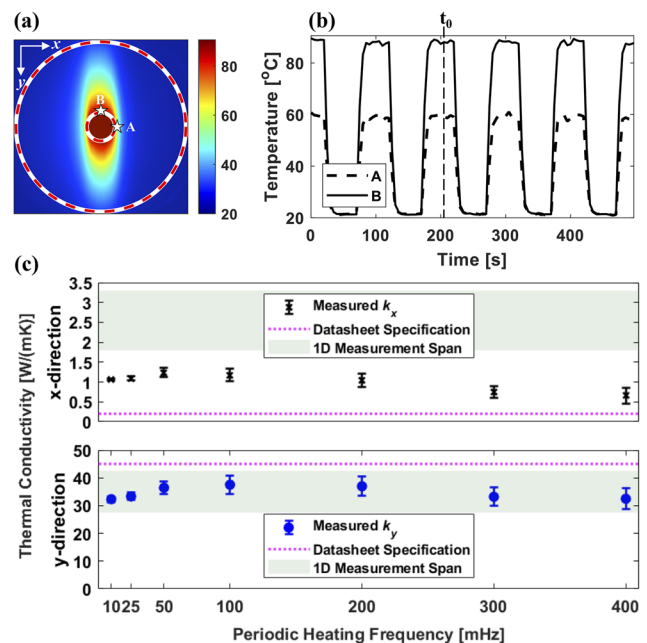


FIG. 9. (a) Two-dimensional temperature distribution on the top surface of the Temprion[®] OHS sample at a time instant t_0 , where the center of the domain attains the highest temperature. (b) The transient temperature response at two discrete locations (Point A outside the right edge of the laser absorber and Point B outside the top edge of the laser absorber). (c) Experimentally measured values of thermal conductivity in the two in-plane orthotropic directions (k_x and k_y) for a $45 \mu\text{m}$ thick sheet of Temprion[®] OHS at various heating frequencies. Both values of k_x and k_y are fit simultaneously in a temperature data set at that particular frequency. The symbols denote the mean thermal conductivity measured at a particular heating frequency, while the error bars denote the uncertainty in the measurement. The dashed magenta dotted lines are the thermal conductivity values from the data sheet, while the shaded green region denotes the range of k as measured by 1D Ångström's method (see the supplementary material, Fig. S2).

the input properties, per the results shown in the supplementary material, Sec. S1.

To independently verify the measured values of k_x and k_y for Temprion[®] OHS using an established technique, narrow strip-like samples were created and characterized using the IR-enhanced one-dimensional version of Ångström's method.²⁸ The measured results are shown in the supplementary material, Fig. S2. Briefly, the measured mean thermal conductivity for a sample cut in the *traverse* direction is $k_x = 2.5 \pm 0.8 \text{ W m}^{-1} \text{ K}^{-1}$, and that for a sample cut in the *machine* direction is $k_y = 37.1 \pm 7.3 \text{ W m}^{-1} \text{ K}^{-1}$. Although the value for k_y , as measured independently using the traditional 1-D Ångström method, matches almost exactly with that measured with the 2-D Laser Ångström method, there is a significant difference in the k_x value. A second 1-D sample measured along the *traverse* direction yielded a thermal conductivity value of $2.0 \pm 0.5 \text{ W m}^{-1} \text{ K}^{-1}$. It is likely that these differences are due to variations in the material properties between the samples or the directional nature of the density and specific heat.

V. CONCLUSION

We have developed and introduced a new technique for the characterization of the in-plane thermal conductivity of both isotropic and anisotropic materials across a wide range of properties and in-plane anisotropy ratios. This technique takes inspiration from the established Ångström method to enable the characterization of thin films and sheets. This measurement implements non-contact infrared imaging and laser heating, and the thermal conductivity of the material is calculated without the measurement of the input heating power, which helps reduce uncertainty. Numerical experiments validated the accuracy of the technique and demonstrated its applicability for both known and hypothetical materials up to high in-plane anisotropy ratios. Another salient feature of this technique is that the thermal conductivity in the two orthotropic directions can be measured simultaneously in a single measurement of one sample, compared to existing techniques that would require preparing multiple samples for each direction of interest. Finally, this measurement technique is demonstrated and validated by conducting experiments using an isotropic reference material, PTFE, and a commercially available anisotropic material, Dupont Temprion[®] Organic Heat Spreader. Through both physical and numerical experiments, it has been demonstrated that this technique can be used to characterize novel materials with very high in-plane anisotropy ratios. The present work validated the technique for materials spanning a range of $0.1\text{--}2000 \text{ W m}^{-1} \text{ K}^{-1}$ and in-plane anisotropy ratios of up to 225, which is higher than most other lock-in thermography techniques and TDTR- and (Frequency-Domain ThermoReflectance) FDTR-based measurement approaches.

This technique is versatile, robust, and straightforward to execute. Other than the application of a thin layer of graphite to increase emissivity if necessary (e.g., for semi-transparent or reflective samples), no special processing of the sample is required before the measurement. The measurement setup could be fabricated using low cost, small form factor infrared cameras (instead of the infrared microscope) and small diode lasers for a compact benchtop system. The additional hardware required to execute experiments using this technique is easily accessible. The metrology tool does not involve

intricate assembly, precise optical alignment, scanning of the laser beam, or deposition of a thin metal transducer layer, unlike some other existing laser-based and pump probe methods. The system can accommodate a wide range of sample properties and geometries. In particular, the frequency of periodic heating is one of the tuning parameters in this technique that allows the characterization of samples across a range of thicknesses. Furthermore, the experimental setup dimensions can be modified to accommodate and measure materials across a wide spectrum of in-plane properties.

Future work should aim to quantify the accuracy and sensitivity of this measurement technique beyond this range with respect to factors such as higher absolute values of thermal conductivity, through-plane and in-plane anisotropy ratios, heating frequency, and material thickness. Improved characterization of heat spreading materials with in-plane anisotropy using this technique can guide material development initiatives and improve the accuracy of thermal designs that utilize such materials.

SUPPLEMENTARY MATERIAL

Additional measurements of the Temprion[®] OHS material and details of the thermal image post-processing steps are provided in the supplementary material document.

ACKNOWLEDGMENTS

The authors would like to thank and acknowledge financial support from the industry members of the Cooling Technologies Research Center (CTRC), a graduated National Science Foundation (NSF) Industry/University Co-operative Research Center at Purdue University. The authors also thank Dr. Jeffrey Meth (DuPont) for providing samples of the Temprion[®] OHS material for measurements as well as for discussions of their behavior and expected material properties.

AUTHOR DECLARATIONS

Conflict of Interest

The authors have no conflicts to disclose.

Author Contributions

Aalok U. Gaitonde: Data curation (equal); Formal analysis (equal); Investigation (equal); Methodology (equal); Validation (equal); Visualization (equal); Writing – original draft (equal); Writing – review & editing (equal). **Aaditya A. Candadai:** Data curation (equal); Formal analysis (equal); Investigation (equal); Methodology (equal); Validation (equal); Visualization (equal); Writing – original draft (equal); Writing – review & editing (equal). **Justin A. Weibel:** Conceptualization (equal); Data curation (equal); Formal analysis (equal); Funding acquisition (equal); Investigation (equal); Methodology (equal); Project administration (equal); Resources (equal); Software (equal); Supervision (equal); Validation (equal); Visualization (equal); Writing – original draft (equal); Writing – review & editing (equal). **Amy M. Marconnet:** Conceptualization (equal); Data curation (equal); Formal analysis (equal); Funding acquisition (equal); Investigation (equal); Methodology (equal); Project administration (equal); Resources (equal); Software (equal); Supervision

(equal); Validation (equal); Visualization (equal); Writing – original draft (equal); Writing – review & editing (equal).

DATA AVAILABILITY

The data that supports the findings of this study are available from the corresponding author upon reasonable request.

REFERENCES

- J. J. de Pablo, N. E. Jackson, M. A. Webb, L. Q. Chen, J. E. Moore, D. Morgan, R. Jacobs, T. Pollock, D. G. Schlom, E. S. Toberer, J. Analytis, I. Dabo, D. M. DeLongchamp, G. A. Fiete, G. M. Grason, G. Hautier, Y. Mo, K. Rajan, E. J. Reed, E. Rodriguez, V. Stevanovic, J. Suntivich, K. Thornton, and J. C. Zhao, “New frontiers for the materials genome initiative,” *npj Comput. Mater.* **5**, 41 (2019).
- A. S. H. Makhlof and N. Y. Abu-Thabit, *Advances in Smart Coatings and Thin Films for Future Industrial and Biomedical Engineering Applications* (Elsevier, 2020).
- G. Mittal, K. Y. Rhee, V. Mišković-Stanković, and D. Hui, “Reinforcements in multi-scale polymer composites: Processing, properties, and applications,” *Composites, Part B* **138**, 122–139 (2018).
- Z.-S. Wu, G. Zhou, L.-C. Yin, W. Ren, F. Li, and H.-M. Cheng, “Graphene/metal oxide composite electrode materials for energy storage,” *Nano Energy* **1**, 107–131 (2012).
- N. Nitta, F. Wu, J. T. Lee, and G. Yushin, “Li-ion battery materials: Present and future,” *Mater. Today* **18**, 252–264 (2015).
- X. Zhang, W. Tan, F. Smail, M. De Volder, N. Fleck, and A. Boies, “High-fidelity characterization on anisotropic thermal conductivity of carbon nanotube sheets and on their effects of thermal enhancement of nanocomposites,” *Nanotechnology* **29**, 365708 (2018).
- X. Qian, J. Zhou, and G. Chen, “Phonon-engineered extreme thermal conductivity materials,” *Nat. Mater.* **20**, 1188–1202 (2021).
- X. Xu, Q. Zhang, M. Hao, Y. Hu, Z. Lin, L. Peng, T. Wang, X. Ren, C. Wang, Z. Zhao, C. Wan, H. Fei, L. Wang, J. Zhu, H. Sun, W. Chen, T. Du, B. Deng, G. J. Cheng, I. Shakir, C. Dames, T. S. Fisher, X. Zhang, H. Li, Y. Huang, and X. Duan, “Double-negative-index ceramic aerogels for thermal superinsulation,” *Science* **363**, 723 (2019).
- R. Shrestha, P. Li, B. Chatterjee, T. Zheng, X. Wu, Z. Liu, T. Luo, S. Choi, K. Hippalgaonkar, M. P. De Boer, and S. Shen, “Crystalline polymer nanofibers with ultra-high strength and thermal conductivity,” *Nat. Commun.* **9**, 1664 (2018).
- G. Xin, H. Sun, T. Hu, H. R. Fard, X. Sun, N. Koratkar, T. Borca-Tasciuc, and J. Lian, “Large-area freestanding graphene paper for superior thermal management,” *Adv. Mater.* **26**, 4521–4526 (2014).
- W. Yu, X. Zhao, P. Jiang, C. Liu, and R. Yang, “Tunable anisotropic thermal transport in super-aligned carbon nanotube films,” *Mater. Today Phys.* **20**, 100447 (2021).
- Z. Luo, J. Maassen, Y. Deng, Y. Du, R. P. Garrelts, M. S. Lundstrom, P. D. Ye, and X. Xu, “Anisotropic in-plane thermal conductivity observed in few-layer black phosphorus,” *Nat. Commun.* **6**, 8572 (2015).
- Y. Guo, Y. Zhou, and Y. Xu, “Engineering polymers with metal-like thermal conductivity—Present status and future perspectives,” *Polymer* **233**, 124168 (2021).
- X. Zhang, X. Chao, L. Lou, J. Fan, Q. Chen, B. Li, L. Ye, and D. Shou, “Personal thermal management by thermally conductive composites: A review,” *Compos. Commun.* **23**, 100595 (2021).
- X. Wang, V. Ho, R. A. Segalman, and D. G. Cahill, “Thermal conductivity of high-modulus polymer fibers,” *Macromolecules* **46**, 4937–4943 (2013).
- C. L. Choy, Y. Fei, and T. G. Xi, “Thermal conductivity of gel-spun polyethylene fibers,” *J. Polym. Sci.* **31**, 365 (1993).
- C. L. Choy, Y. W. Wong, G. W. Yang, and T. Kanamoto, “Elastic modulus and thermal conductivity of ultradrawn polyethylene,” *J. Polym. Sci., Part B: Polym. Phys.* **37**, 3359–3367 (1999).
- Y. Xu, D. Kraemer, B. Song, Z. Jiang, J. Zhou, J. Loomis, J. Wang, M. Li, H. Ghasemi, X. Huang, X. Li, and G. Chen, “Nanostructured polymer films with metal-like thermal conductivity,” *Nat. Commun.* **10**, 1771 (2019).
- A. A. Candadai, J. A. Weibel, and A. M. Marconnet, “Thermal conductivity of ultrahigh molecular weight polyethylene: From fibers to fabrics,” *ACS Appl. Polym. Mater.* **2**, 437–447 (2020).
- J. P. Feser, J. Liu, and D. G. Cahill, “Pump-probe measurements of the thermal conductivity tensor for materials lacking in-plane symmetry,” *Rev. Sci. Instrum.* **85**, 104903 (2014).
- P. Jiang, X. Qian, and R. Yang, “A new elliptical-beam method based on time-domain thermoreflectance (TDTR) to measure the in-plane anisotropic thermal conductivity and its comparison with the beam-offset method,” *Rev. Sci. Instrum.* **89**, 094902 (2018).
- J. W. Vandersande and R. O. Pohl, “Simple apparatus for the measurement of thermal diffusivity between 80–500 K using the modified Ångström method,” *Rev. Sci. Instrum.* **51**, 1694–1699 (1980).
- A. J. Ångström, “New method of determining the thermal conductivity of bodies,” *London, Edinburgh Dublin Philos. Mag. J. Sci.* **25**, 130–142 (1863).
- W. J. Parker, R. J. Jenkins, C. P. Butler, and G. L. Abbott, “Flash method of determining thermal diffusivity, heat capacity, and thermal conductivity,” *J. Appl. Phys.* **32**, 1679–1684 (1961).
- S. Lee and D. Kim, “The evaluation of cross-plane/in-plane thermal diffusivity using laser flash apparatus,” *Thermochim. Acta* **653**, 126–132 (2017).
- G. Forte and S. Ronca, “Laser-flash in-plane thermal analysis: The case of oriented UHMWPE,” *AIP Conf. Proc.* **1736**(1), 020171 (2016).
- F. Cernuschi, A. Russo, L. Lorenzoni, and A. Figari, “In-plane thermal diffusivity evaluation by infrared thermography,” *Rev. Sci. Instrum.* **72**(10), 3988–3995 (2001).
- J. Hahn, T. Reid, and A. M. Marconnet, “Infrared microscopy enhanced Ångström’s method for thermal diffusivity of polymer monofilaments and films,” *J. Heat Transfer* **141**(8), 081601 (2019).
- K. Kim, P. J. Kim, R. A. Chowdhury, R. Kantharaj, A. Candadai, A. Marconnet, V. G. Pol, and J. P. Youngblood, “Structural orientation effect of cellulose nanocrystals (CNC) films on electrochemical kinetics and stability in lithium-ion batteries,” *Chem. Eng. J.* **417**, 128128 (2021).
- Y. Hu and T. S. Fisher, “Accurate thermal diffusivity measurements using a modified Ångström’s method with Bayesian statistics,” *J. Heat Transfer* **142**(7), 071401 (2020).
- C. S. Welch, D. M. Heath, and W. P. Winfree, “Remote measurement of in-plane diffusivity components in plates,” *J. Appl. Phys.* **61**, 895–898 (1987).
- L. Perez and L. Autrique, “Robust determination of thermal diffusivity values from periodic heating data,” *Inverse Probl.* **25**, 045011 (2009).
- A. Mendioroz, R. Fuente-Dacal, E. Apiñaniz, and A. Salazar, “Thermal diffusivity measurements of thin plates and filaments using lock-in thermography,” *Rev. Sci. Instrum.* **80**, 074904 (2009).
- H. Kato, T. Baba, and M. Okaji, “Anisotropic thermal-diffusivity measurements by a new laser-spot-heating technique,” *Meas. Sci. Technol.* **12**, 2074–2080 (2001).
- L. Tang and C. Dames, “Anisotropic thermal conductivity tensor measurements using beam-offset frequency domain thermoreflectance (BO-FDTR) for materials lacking in-plane symmetry,” *Int. J. Heat Mass Transfer* **164**, 120600 (2021).
- P. Jiang, B. Huang, and Y. K. Koh, “Accurate measurements of cross-plane thermal conductivity of thin films by dual-frequency time-domain thermoreflectance (TDTR),” *Rev. Sci. Instrum.* **87**, 075101 (2016).
- S. Sandell, E. Chávez-Ángel, A. El Sacht, J. He, C. M. Sotomayor Torres, and J. Maire, “Thermoreflectance techniques and Raman thermometry for thermal property characterization of nanostructures,” *J. Appl. Phys.* **128**, 131101 (2020).
- I. C. Christov, R. J. Decker, A. Demirkaya, V. A. Gani, P. G. Kevrekidis, and R. V. Radomskiy, “Long-range interactions of kinks,” *Phys. Rev. D* **99**(1), 016101 (2019).
- DuPont, Tempriion[®] OHS—organic heat spreader, <https://www.dupont.com/products/tempriion-ohs.html>, 2022.
- D. M. Price and M. Jarratt, “Thermal conductivity of PTFE and PTFE composites,” *Thermochim. Acta* **392–393**, 231–236 (2002).
- K.-L. Hsu, D. E. Kline, and J. N. Tomlinson, “Thermal conductivity of polytetrafluoroethylene,” *J. Appl. Polym. Sci.* **9**, 3567–3574 (1965).

⁴²A. U. Gaitonde, “Thermal transport in lithium ion batteries: An experimental investigation of interfaces and granular materials,” M.S. thesis, School of Mechanical Engineering, Purdue University, West Lafayette, 2016.

⁴³A. U. Gaitonde, A. Nimmagada, and A. M. Marconnet, “Experimental characterization of thermal conductance across the separator-shell interface in dry cylindrical lithium ion batteries,” in Intersociety Conference on Thermal and Thermomechanical Phenomena in Electronic Systems (ITherm), 2017.

⁴⁴A. U. Gaitonde, A. Nimmagadda, and A. M. Marconnet, “Measurement of interfacial thermal conductance in lithium ion batteries,” *J. Power Sources* **343**, 431–436 (2017).

⁴⁵R. Kantharaj, I. Srivastava, K. R. Thaker, T. S. Fisher, A. U. Gaitonde, A. Bruce, J. Howarter, and A. M. Marconnet, “Thermal conduction in graphite flake-epoxy composites using infrared microscopy,” in Intersociety Conference on Thermal and Thermomechanical Phenomena in Electronic Systems (ITherm), 2017.

⁴⁶J. Meth, DuPont, personal communication (2021).